Construction and Building Materials 509 (2026) 145199

Contents lists available at ScienceDirect

Construction and Building Materials

journal homepage: www.elsevier.com/locate/conbuildmat

Engineered bicomponent polypropylene fibers: Effects of mineral particles on spinnability, surface roughness, mechanical strength, and adhesion in cementitious matrices

Mihaela-Monica Popa [a], Cesare Signorini [b], Norbert Smolka [a], Viktor Mechtcherine [b], Christina Scheffler [a,b,*]

[a] Leibniz-Institut für Polymerforschung Dresden e. V. (IPF), Dresden, Germany
[b] TU Dresden, Institute of Construction Materials, Dresden 01062, Germany

A R T I C L E I N F O

Keywords:
Polypropylene fibers
Bicomponent fibers
Melt-spinning
Fiber surface micro roughness
Interfacial interlocking

ABSTRACT

Polypropylene (PP) fibers are widely used in fiber-reinforced concrete (FRC) and Strain-Hardening Cement-based Composites (SHCCs), to improve crack control, reduce plastic shrinkage cracking, and enhance ductility. However, their smooth surface and low chemical reactivity limit fiber-matrix interaction. The goal of this research is to develop engineered core-shell bicomponent PP fibers and improve their interfacial adhesion with cement-based binders by gradually increasing the amount of fine ground calcium carbonate (GCC) powder in the fiber shell. The influence of stepwise increasing GCC content on fiber spinnability, surface micro-roughness, and tensile strength, was assessed to optimize the particle content for stable and continuous spinning. Differential Scanning Calorimetry (DSC) revealed that GCC hinders the dynamic crystallization and affects the melting temperature, potentially influencing melt-spinning by altering flow behavior and solidification kinetics. Single fiber pullout (SFPO) tests demonstrated that fibers with optimized GCC content exhibited higher energy absorption due to increased surface micro-roughness, promoting mechanical interlocking with the matrix, as confirmed by scanning electron microscope (SEM) observations of localized matrix deformation. The SEM observations also suggested that GCC particles promote cementitious hydration phase growth after immersion in the cement solution. A threshold particle content of 20 vol% marked the transition from pullout-dominated to partial fiber breakage, while higher contents led to premature fiber rupture. These results demonstrate that GCC-induced surface roughness can effectively enhance microscale fiber–matrix interactions and energy dissipation during pullout.

1. Introduction

Recent research has focused on enhancing the tensile ductility of Strain-Hardening Cementitious Composites (SHCC) by comprehending and optimizing the fiber crack-bridging mechanisms, with the goal of improving the performance of the material under various loading conditions [1–3]. This goal can be pursued by adjusting the matrix composition, for example by replacing Portland cement with alternative pozzolanic materials with reduced environmental impact such as calcium carbonate ($CaCO_3$) particles, and by modifying the fiber surface to increase its roughness or hydrophilicity. The mechanical properties of SHCCs and the fiber-matrix interaction at the micro level have been acknowledged to greatly influence the properties of the composites at macroscopic level, as highlighted by Kanda and Li [4] and Ranade *et al.* [5], are prone to vary their effects at different strain ratios [6].

Fibers commonly used in SHCC, such as polyethylene (PE), polyvinyl alcohol (PVA), polyvinyl chloride (PVC), and polypropylene (PP), are known for their resistance to chemical degradation in highly alkaline environments. Within this wide spectrum, PP fibers are emerging as a promising reinforcement option due to their cost-effectiveness, durability, high degree of recyclability [7,8] and established use in concrete [9,10]. However, the flammability of PP fibers represents a considerable drawback stemming from their wholly aliphatic hydrocarbon structure [11]. In addition, the inert chemical nature and smooth surface of PP fibers limit the adhesion with hydraulic matrices, thus impairing their crack-bridging ability.

---

* Corresponding author at: Leibniz-Institut für Polymerforschung Dresden e. V. (IPF), Dresden, Germany.
E-mail address: scheffler@ipfdd.de (C. Scheffler).

https://doi.org/10.1016/j.conbuildmat.2026.145199
Received 28 June 2025; Received in revised form 7 January 2026; Accepted 8 January 2026

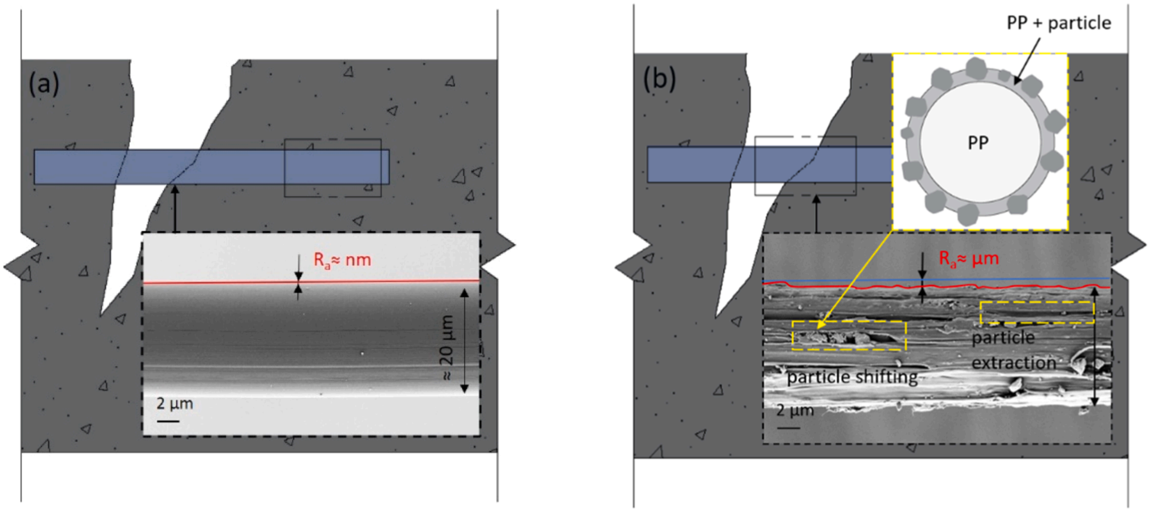

Fig. 1. Performance-based design of PP fibers: (a) monocomponent PP fiber with minimal surface micro-roughness and (b) bicomponent PP fiber with high surface micro-roughness and representative cases of fiber deformation during crack propagation. The top-right inlet of (b) shows the schematic of the morphology of the particles.

As a novel approach that deviates from the traditional concepts of fiber coating or etching, bicomponent and blended PP fibers incorporating different particles, have been produced by melt-spinning to explore their potential and properties for a large spectrum of applications. In particular, the effect of melt-spinning processing parameters on the thermal, physical, and mechanical properties of PP fibers/yarns containing Phase Change Materials (PCMs) has been investigated. These PCMs include granular shells of melamine-formaldehyde resin and paraffin waxes [11–14], and granular particles with melamine-formaldehyde capsule including either paraffin [13] or microencapsulated flame retardant [11] cores. In particular, Salaün *et al.* [11] examined the feasibility of adopting these materials in textile applications. In addition, the influence of size and shape of $CaCO_3$ particles added to PP fibers as a blend was studied with respect to spin-line limitation, stability, fiber forming structure, rheology, and mechanical properties. Ground $CaCO_3$ particles (mean size 2.2 µm) and precipitate $CaCO_3$ particles (mean sizes ranging from 0.25 to 1.1 µm and 0.7 µm) have been investigated as blends with PP resin. The study compared the effects of different filler concentrations including 5, 10, 15 and 20 wt% [15]. Ariffin *et al.* [16] alternatively blended 30 wt% $CaCO_3$ (mean size 4.5 µm) and talc (mean size 6.3 µm) and studied the particle content limitation before fracture. Based on observations from both studies, the die swell ratio and degree of melt fracture for multicomponent-filled PP are generally lower than for $CaCO_3$-filled PP but higher than for talcum-filled PP.

Previous studies by the authors focused on manufacturing bicomponent PP fibers using a melt-spinning process [17–21] as illustrated in Fig. 1. Rice-shaped Precipitated Calcium Carbonate (PCC) particles with particle size volume median diameter (VMD) width of 4.07 ± 0.44 µm were incorporated into the fiber shell up to 10 vol% to enhance the surface micro roughness for better mechanical interlocking with the cementitious matrix. Although single-fiber micromechanical pullout tests showed twice the pullout work compared to commercial PP monocomponent fibers, particle agglomeration occasionally caused fiber rupture during spinning, limiting their processability.

To address these processing issues, the current study focuses specifically on replacing PCC with Ground Calcium Carbonate (GCC), which has a smaller particle size, different morphology (size and shape) and reduced agglomeration. The aim is to refine the design of PP fibers by incorporating GCC-coated powder with an even finer particle size in the outer layer, in order to achieve better melt-spinning stability than in earlier studies [19]. The upper limit of particle content in the outer shell will also be determined, with the aim of further improving the interfacial bonding with a fine-grained cementitious matrix, focusing mainly on the pullout behavior. Although GCC particles could potentially interact chemically with cement hydration products, the present study focuses on mechanical interlocking as the main reinforcement mechanism. The filament core is designed to contribute to fiber strength. At the same time, the particle size is crucial for the processability (compounding and melt-spinning steps), which is constrained by technical parameters such as spin-die size, with the drawing stage limited compared to pure PP fibers without particles.

One of these GCC-based fiber formulations was up-scaled and incorporated into specially designed limestone calcined clay cement (LC^3)-based composites, showing favorable mechanical interlocking properties for application in highly tough fiber-reinforced cementitious composites [21]. In fact, it is known that interfacial properties must be precisely adjusted to prevent easy extraction when bond stress is too low. Additionally, the fiber-matrix bond should not exceed a certain threshold, as this can result in easy tensile failure and limited toughness [22]. At the composite scale, these fibers enhanced fiber–matrix interlocking, improving the fresh and hardened properties of limestone calcined clay cement (LC^3)-based composites with a low cement content of 35 % by weight of the total binder, allowing a significant reduction of the fiber dosage (2.5 vol%) while matching or even surpassing the mechanical performance obtained with 3 vol%. of commercial monocomponent PP fibers. Additionally, dynamic tensile tests supported this outcome, showing that the PP fibers with improved interfacial properties ensured satisfactory toughness and triggered multiple cracking patterns in fiber-reinforced concrete [23]. This study focuses on the microscopic evaluation of the new fibers developed, which includes examining GCC particles, fiber surface roughness, and conducting micro-mechanical tests such as single fiber tensile and pullout tests. The study also explores nucleation and growth mechanisms on PP fiber surfaces in a cementitious solution, considering a sort of commercial monocomponent PP fiber as a benchmark.

2. Materials and methods

2.1. Materials

Monofilament bicomponent fibers could be manufactured at IPF using a commercially available polypropylene grade (PP: HG 475 FB, Borealis, Vienna, Austria). The as-received virgin PP was used as the

Table 1
Matrix composition (dosages are given in kg/m^3).

Raw constituent / Product	Supplier	Dosage
Portland cement CEM I 42.5 R-HS	Schwenk, Germany	505
Fly ash Steament H4	Steag Power Minerals, Germany	621
Quartz sand 0.06–0.2 mm	Strobel Quarzsand, Germany	536
Superplasticizer Master Glenium ACE 30	BASF, Germany	10
Viscosity modifying agent (VMA)	SIKA, Switzerland	4.8
Water		338

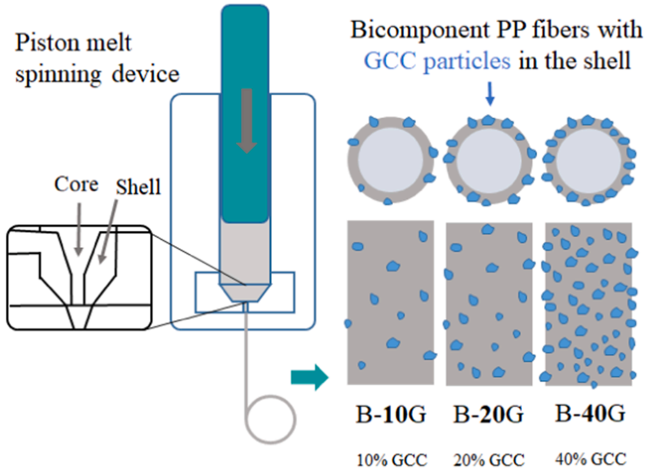

Fig. 2. Simplified schematic representation of the spinning process including GCC particles.

Table 2
Overview of investigated fibers; parameters and flowability rate property for bicomponent fiber manufacturing.

Fiber type	Shell composition	Shell *MFR* g/10 min	Fiber name	Core *MFR* g/10 min
Monocomponent fiber (M), commercial	–	–	M-PP – Commercial)	–
Bicomponent fiber (B)	PP + 10 vol% GCC	70.93	B-10G	29.29
	PP + 20 vol% GCC	61.30	B-20G	
	PP + 40 vol% GCC	40.57	B-40G	

core and shell material for all fibers. Different volume percentages of GCC particles supplied by Omya (Oftringen, Switzerland) were mixed with the PP by a microcompounder (Xplore Instruments B.V. 5&15 Micro Compounder, Sittard, The Netherlands) to produce the material mix for the shell. The polymer mixture was prepared to obtain a homogeneous mix following the same procedure as in the investigations of Popa *et al.* [19] in batches of 16 g, at 230 °C, for 10 min, at a rotor speed of 100 rpm. In addition, the shell material was pelletized to facilitate the melt-spinning process. For a better comparison, the cementitious matrix developed by Curosu *et al.* [6] and recalled in Table 1 was used for single fiber pullout (SFPO) tests to evaluate the interfacial adhesion between fiber and matrix.

2.2. Methods

2.2.1. Monofilament bicomponent fiber processing technology

Individual core-shell bicomponent PP fibers were produced using a piston spinning device designed and built at the IPF [24], with two chambers, each with a volume of 10 cm^3. These fibers consist of two components arranged in a core-shell configuration. The core component acts as the structural backbone for the unstable shell material, hence contributing to the fiber stability and strength [25].

The pellets were melted in two separate piston chambers and pressurized into the die, which put together the melt streams into a thin bicomponent single filament stream, allowing the core-shell ratio to be adjusted at a temperature of 220°C. The total mass flow rate of the bicomponent fiber production was 1.25 cm^3/min. The diameters of the die (nozzle holes) were 0.5 mm for the core and 0.8 mm for the shell, with a chosen core-shell ratio of 80/20 %. After spinning, the filaments were wound onto a bobbin at a maximum winding speed of 800 m/min and spooled in a free-fall section. An offline drawing ratio of three (DR=3) was applied by stretching single filaments using a Zwick/Roell Z0.5 (Ulm, Germany) tensile testing device. The gauge length was set to 100 mm, with a pre-test displacement rate of 500 mm/min and a drawing displacement rate of 200 mm/min. Fig. 2 illustrates a schematic of the fiber spinning workflow.

For a more comprehensive comparison of their interaction with the concrete matrix, the bicomponent PP fibers investigated in this study, which feature different surface micro roughness, were evaluated taking into account the results of previous studies [20]. Furthermore, commercially available monocomponent PP fiber sourced from Baumhueter GmbH (Rheda-Wiedenbrück, Germany) were considered as a benchmark. Technical and morphological details on the features of the fiber shells are detailed in Table 2. Three different dosages of GCC particles in the shell of bicomponent fibers were investigated, namely 10 %, 20 % and 40 % by volume. The melt flow rate (*MFR*) of the core and shell materials were determined according to ISO 1133 at 230°C/2.16 kg. The core *MFR* of PP: HG 475 FB closely aligns with the value of 27 g/10 min provided by the supplier. However, during compounding, the high temperatures cause the polymer chains in PP to break, resulting in shorter chains, which increases the *MFR* and improves flowability compared to pure PP. However, as the GCC particle content increases, the proportion of PP in the sample decreases. This reduction in PP leads to a higher filler-to-polymer ratio, which typically lowers flowability. Furthermore, the GCC particles may form agglomerates, which restrict the mobility of the polymer chains and increase the system's viscosity, ultimately decreasing the overall flowability as particle content continues to rise. Additionally, the unknown coating on the GCC particles may also influence the overall system and its properties.

2.2.2. Particle size distribution, bicomponent PP fiber morphology and micro roughness measurements

The as-received GCC particle size distribution analysis was determined using a laser diffraction with a Helos/BR particle size analyzer equipped with a RODOS dry dispersion unit and ASPIROS microdose module (Sympatec, Clausthal-Zellerfeld, Germany). The measurements were conducted at a pressure of 1 bar pressure. The cumulative particle distribution provides values for $d_{v,10}$, $d_{v,50}$, and $d_{v,90}$, representing the diameters at which 10 %, 50 %, and 90 % of the GCC are included, respectively. The particle size volume median diameter (VMD), reflected by the median diameter ($d_{v,50}$), offers an average particle size based on volume distribution.

Differential scanning calorimetry (DSC) was employed to examine how the crystallization properties of the polymer compounds might impact further spinning process, as the content of GCC fine powder in the fiber shell was incrementally increased. The samples, tested in a nitrogen atmosphere using a DSC Q2000 (TA Instruments, USA), underwent heating at a rate of 10 °C/min 220°C (1st run), followed by cooling and reheating at the same rate (2nd run) while recording heat flow. Crystallinity was determined using a melting enthalpy (ΔH_{lit}, 100 % = 207 J/g) for PP as referenced in [19].

Scanning electron microscopy (SEM) analyses were conducted at

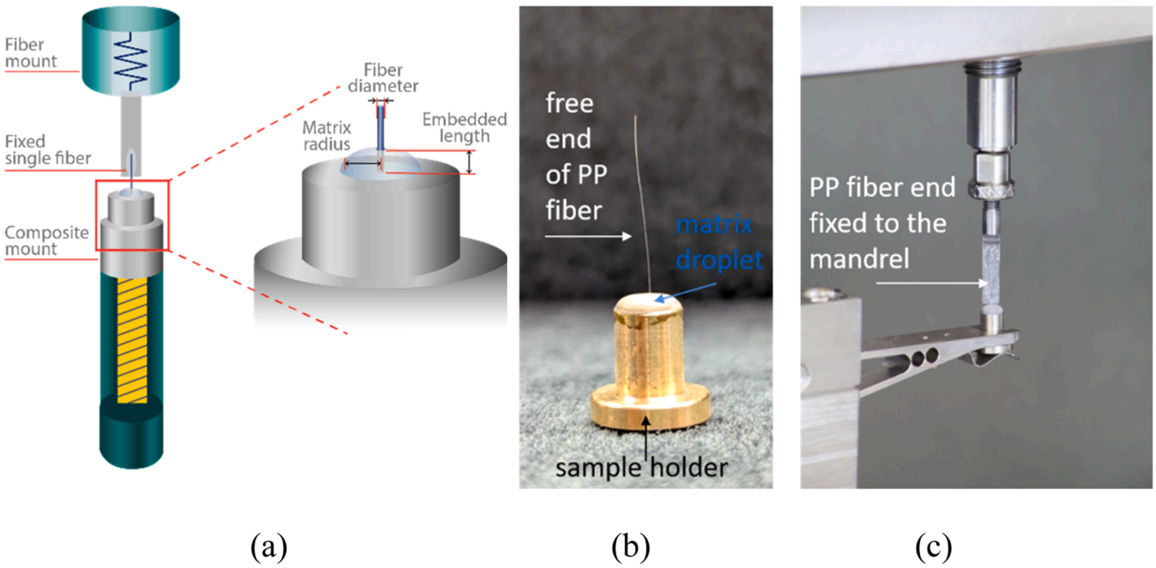

(a) (b) (c)

Fig. 3. Single-fiber pullout test: (a) a schematic of the setup, (b) single fiber embedded in the matrix prior to testing, and (c) pullout test setup with the sample mounted into the testing device with the free fiber end fixed to the mandrel using an adhesive.

various magnifications using a Carl Zeiss Microscopy GmbH ULTRA PLUS microscope equipped with a secondary electron (SE) detector to examine filament morphology and particle distribution along the fiber shell and cross-sectional areas. To prevent charging effects due to the insulating nature of PP, the samples were coated with Pt-Pd prior to analysis. SEM analysis was also employed to examine the surface modification of the individual polypropylene (PP) fibers after immersion in a cementitious pore solution under different time step conditions in order to observe potential growth of mineral phases initiated by the GCC particles. Cement (CEM I 42.5R-HS) was initially mixed with tap water at 23°C for 72 h. The M-PP fiber with a diameter of 19.8 µm and the B-20G PP fiber with a diameter of 22.7 ± 0.4 µm were specifically chosen for analysis. Following CEM filtration, these fibers were transferred into a sample holder and subjected to immersion time periods ranging from 24 h to 5 days. Post-removal from the sample holders, the fibers underwent rinsing with deionized water, drying at room temperature, and subsequent preparation and analysis via SEM.

Micro roughness was quantitatively assessed using a confocal microscopy (µSurf expert, Nanofocus AG, Oberhausen, Germany). Correlations between surface morphology and topography (micro roughness) of hydrophobic bicomponent PP fiber surfaces were established using a 50 × magnification objective, capturing images of 320 µm× 320 µm with a resolution of 1024 × 1024 pixels. The sampling interval was adjusted based on the dominant scale of different parts of the analyzed surface. Additionally, the µSoft analysis software was employed to adjust the cylindrical shape of the fibers. However, areas with abrupt slopes could not be avoided, causing the microscope light to improperly capture the surface points, which may introduce errors in the roughness analysis, based on 3D surface profiles. Micro roughness analysis included arithmetic mean deviation of the surface, S_a, and the ten-point height of the surface, S_z [26] of the flattened fiber surface was performed on different selected areas along the fiber axis. Data analysis included repeated measurements on a minimum of ten fibers per composition.

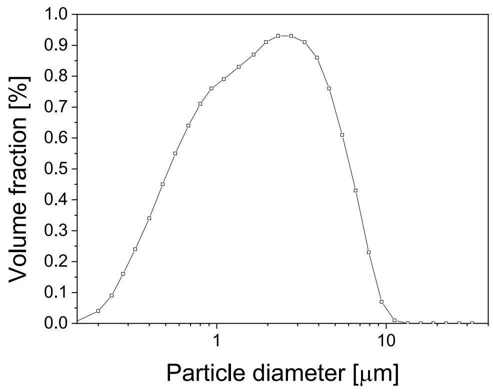

Fig. 4. Monomodal particle size distribution of as-received GCC microparticles.

2.2.3. *Tensile testing for single fibers*

Single-fiber tensile tests were conducted on the bicomponent PP fibers to determine their tensile strength and Young's modulus. The tests were performed using a FAVIMAT+ machine (Textechno H. Stein GmbH & Co. KG, Germany) equipped with a 610 cN load cell and hard rubber/vulkolan clamps. Prior to testing, fiber diameter was determined on a fixed length scale of 50 mm using a vibroscopy system, and was calculated using a density of 0.9 g/cm^3. Each fiber was clamped at an initial length of 100 mm and tested at a rate of 5 mm/min under standard room conditions (23°C, 50 % relative humidity). The linear density of each individual fiber, required for the evaluation, was determined prior to the tensile test using the vibroscopic method in accordance with ASTM D1577 [27] guidelines. From this, the diameter of each fiber was calculated, assuming a density of 0.9 g/cm^3 for PP. To ensure accuracy, stress-strain curves were recorded for a minimum of 30 samples per composition.

2.2.4. *Single fiber pullout test*

The effects of micro-GCC particle addition on the bonding performance of the bicomponent PP fibers embedded in a concrete composite were investigated by single fiber pullout (SFPO) tests, as illustrated in Fig. 3. As in our previous studies [17,24], the cementitious matrix was prepared using a high-speed mixer, and single fibers were embedded into the matrix at a constant speed to a depth of approximately 1000 µm with computer assistance. After curing for 28 days at a relative humidity of 97–99 %, a cyanoacrylate adhesive was used to fix one end of the fiber to a mandrel.

SFPO tests were then conducted at a pulling speed of 10 mm/s and a strain rate of 10 s^{-1}, as recommended by Wölfel *et al.* [28], and the force-displacement curves were obtained. SFPO test was possible for displacements up to 450 µm due to the technical limitations of the piezo-actuator adopted. As a consequence, force-displacement curves

Table 3
The particle size distribution fraction values were derived through particle size distribution analysis.

Material	$d_{v,10}$ [μm]	$d_{v,50}$ [μm]	$d_{v,90}$ [μm]	VMD [μm]	Span factor [-]
GCC	0.51 ± 0.01	1.78 ± 0.02	5.12 ± 9.94	2.37 ± 0.02	1.30

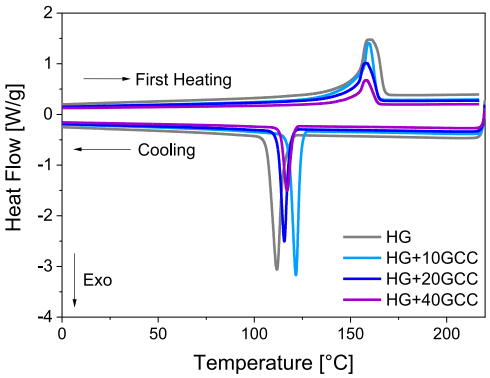

Fig. 5. DSC curves of the PP sample (HG) used to calibrate the heat of fusion vs. the compounded materials.

were evaluated as energy absorption (W_{total}) up to the maximum displacement of 300 μm, as defined in Eq. 1, to ensure a constant strain rate during the test. At least 15 single fibers of each type were analyzed to ensure the necessary statistical rigor.

$$W_{total} = \int_{0}^{l_e} F(s)ds \tag{1}$$

3. Results and discussion

3.1. Particle size distribution analysis

Fig. 4 shows the GCC particle size distribution, measured using a confocal laser scanning diffractometer (LCD) and the main information is summarized in Table 3. The monomodal distribution ranges from 0.13 μm to 11.16 μm, with cumulative volume-based size distribution values aligning with the expected size range. The narrower distribution, indicated by smaller span values, reflects a tighter range of particle sizes, which could influence the flowability of the compound during melt-spinning. The span factor, measured according to British Standards [29] and Chew and Chan [30], quantifies the width of the distribution, further confirming the narrow spread of the particle sizes. In the melt-spinning process, GCC particles are concentrated in the shell of the fiber (20 %), while the core remains pure polymer. Although the narrow particle distribution helps prevent die clogging, the high standard deviation in $d_{v,90}$ indicates the presence of larger particles or potential agglomerations.

These could disrupt the uniform dispersion within the shell, creating weak points that may lead to premature fiber breakage and reduced tensile strength. Improving particle size uniformity and dispersion is essential for enhancing fiber quality and performance.

3.2. Thermal analysis of raw PP and compounds

The impact of chain alignment in raw PP versus compounds with 10 %, 20 % and 40 % GCC particles by volume fractions were investigated using differential scanning calorimetry (DSC), as shown in Fig. 5.

The DSC results (Fig. 6) show that GCC particles had no significant effect on the melting temperature of the compounds, consistent with Zuiderduin *et al.*'s findings [31]. While the 10 vol% GCC sample showed a slight decrease in ΔH_m and X_c, possibly due to sample inhomogeneity, the 20 and 40 vol% samples exhibited values similar to as-received PP. This suggests that the polymer chains remained largely intact during compounding at 230°C, with no significant thermal degradation occurring, as indicated by Gonzalez *et al.* [32]. The slightly increased ΔH_m and X_c in these compounds might be attributed to the nucleating effect of GCC, as noted by Al-Samhan *et al.* [33] and Mao *et al.* [34].

As known from previous work with fibers showing a core-shell ratio of 80/20, the particles are placed close to the fiber surface, partly being exposed. Their localization at the very outside of the cross-section suggests that the crystallization and polymer alignment inside the fiber core is less effected by the particles. During melt-spinning, the crystalline structure requires almost same energy to melt, enabling consistent polymer flow and fiber formation. Based on the DSC results it can be stated that the reduced spinnability of fibers with increasing particle content seems to be less a consequence of reduced chain alignment but instead of geometrical factors caused by hindering the particles when flowing through and leaving the nozzle. However, the Young`s Modulus (see part 3.4), that is strongly depending on the chain alignment and degree of crystallinity, is reducing with increasing particle content, what is contradicting this assumption and highlights the demand for further investigation.

3.3. Surface, cross-sectional area, morphology, and roughness of bicomponent PP fibers

The SEM morphology images in Fig. 7 depict the surface of B-PP fibers containing particles in their shell after offline drawing, compared to M-PP fibers. In all cases, the core of B-PP fibers (Fig. 7b-d) is fully covered by a shell layer consisting of PP and GCC particles, resulting in a significantly rougher surface than the as-received M-PP fibers (Fig. 7a). In addition, the surface roughness is considerably affected by the extent

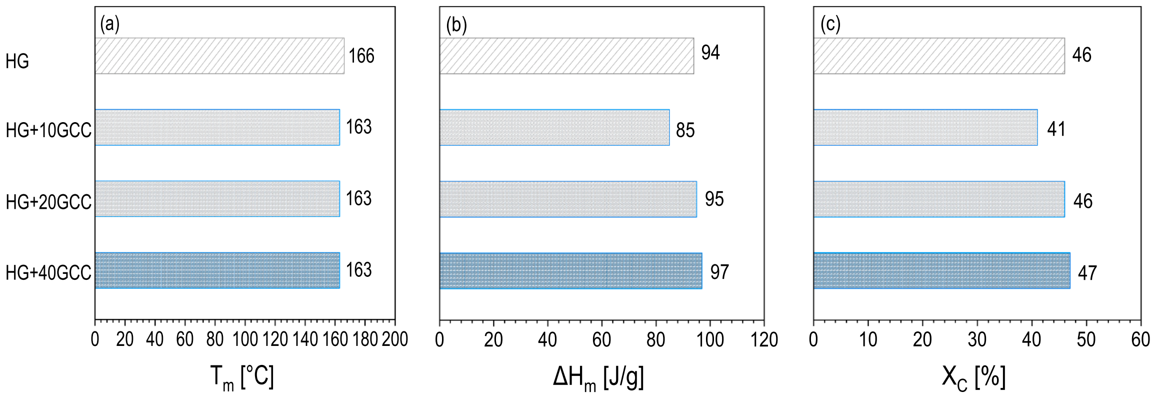

Fig. 6. Thermal properties of PP and compounded materials with varying concentrations of GCC particles.

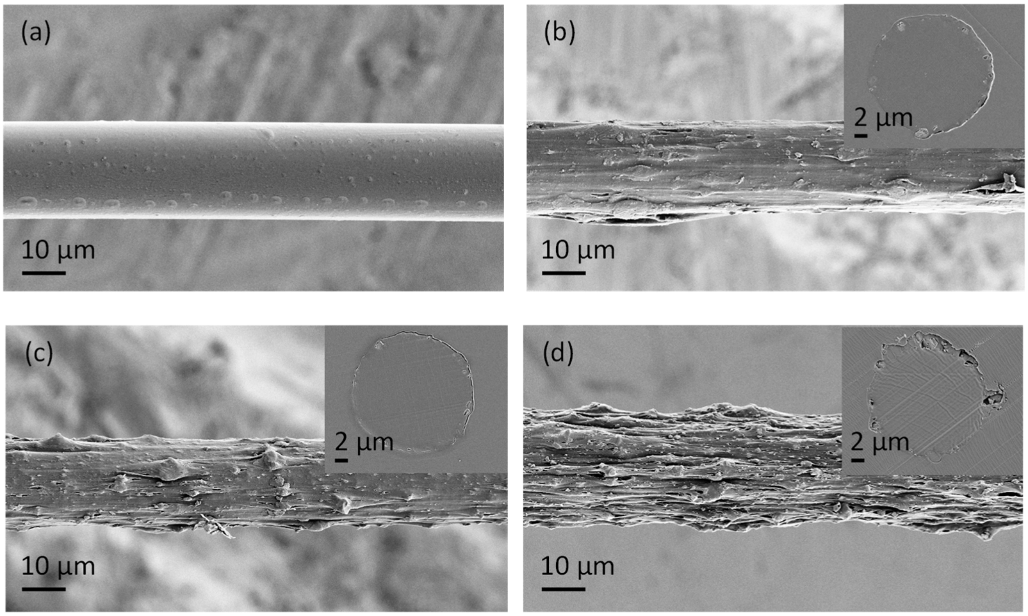

Fig. 7. SEM representative images of surface morphology along the fiber axis and cross-sectional areas of (a) M-PP fiber vs. the offline drawn (DR=3) (b) B-10G, (c) B-20G and (d) B-40G PP fibers.

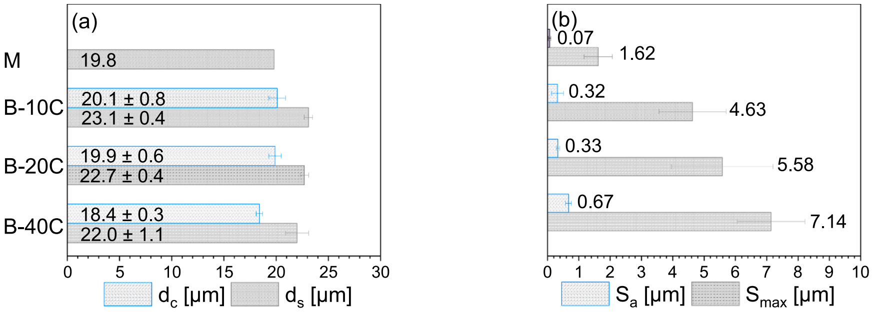

Fig. 8. Bar graphs illustrating the (a) shell ds (blue charts) vs. core dc (gray charts) diameters and (b) mean values of the arithmetic mean deviation of the surface Sa (blue charts) and ten-point height of the surface Smax (gray charts) and the standard deviations values of the M-PP fiber vs. the offline drawn (DR=3) B-10G, B-20G and B-40G PP fibers determined by confocal microscopy. Note the different limits of the scale axes.

of particle addition and increases with increasing particle amounts.

Further texture morphology analysis on the cross-section of the B-10G, B-20G, and B-40G PP fibers confirmed the successful integration of the GCC particles into the outer layer. However, large particle sizes and subsequent agglomerations observed in the SEM images, particularly at higher GCC concentrations, pose manufacturing challenges. These agglomerations can disrupt the spinning process, increasing the risk of filter blockage and die clogging during extrusion. During melt spinning, fibers with lower GCC content (B-10G) demonstrated smoother processing and fewer disruptions (e.g. breakage during offline drawing), correlating with the more uniform dispersion observed in Fig. 7b. In contrast, higher GCC concentrations (B-20G and B-40G) resulted in noticeable inconsistencies during spinning, likely caused by the increased particle content and agglomerations, which created localized flow disruptions. This behavior emphasizes the critical role of proper particle amount and dispersion in maintaining stable spinning conditions and producing defect-free fibers.

Fig. 8a displays the diameters of bicomponent PP fibers analyzed using SEM, while the diameter of commercial monocomponent PP fiber was provided by the supplier. Fig. 8b presents the micro roughness measurement of B-PP fibers in comparison with smooth M-PP fibers, which exhibit very low average micro roughness. The S_a and S_z parameters, as outlined in Fig. 8b, describe surface roughness properties as defined by Stout *et al.* [35]. S_z values may be more suitable for evaluating mechanical interlocking in concrete, as it quantifies the absolute height differences between the peaks and valleys, reflecting the surface's potential for strong interlocking with the concrete matrix, which is essential for enhancing fiber adhesion for micro crack bridging, and overall mechanical performance. Fibers containing 10 vol% GCC particles exhibited an average micro roughness ($S_z = 4.63 \pm 1.07$ µm), slightly different to that of fibers with the same amount of PCC particles ($S_z = 3.67 \pm 0.96$ µm) [19]. This difference might be due to the presence of larger GCC particles, even PCC fillers, which tend to form agglomerates that might not have been fully detected within the selected surface areas for this analysis. In our previous work [19], these larger particles or agglomerates led to an unstable melt-spinning process, setting 10 vol% as the upper limit for PCC content compared to the use of GCC in this study. Interestingly, no significant increase in surface micro roughness was captured up to 20 vol% when S_a values are considered, despite the potential for higher particle concentrations to alter polymer melt flow. However, above this threshold (B-40G PP fiber) notable amplification in micro roughness, approximately twice that of the other counterparts was indicated. The 10, 20 and 40 vol% thresholds were arbitrarily chosen for the bicomponent PP fiber production. Continuous spinning was not achieved at this level, with fibers breaking after only a few meters, preventing upscaling and highlighting

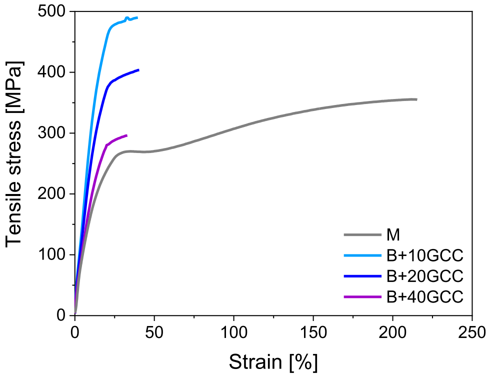

Fig. 9. Tensile stress-strain curves of the M-PP fiber vs. the offline drawn (DR=3) B-PP fibers.

challenges in achieving consistent spinnability at higher filler concentrations.

Other investigation techniques could have been adopted to characterize the variation in surface properties of bicomponent PP fibers compared to commercial counterparts. Water contact angle measurement, for example, is a direct indicator of wettability and is widely used, especially when chemical treatments are performed. Although contact angle measurements were performed in this study, the fibers' pronounced surface roughness led to a strong hysteresis in thereby impairing the formation of a clear contact line [36]. The significant scatter associated with this measurement prevented meaningful interpretation of the data and could lead to misleading conclusions. In fact, other studies in the literature could quantify the change in wettability compared to the reference PP fiber or membrane only for roughness extents in the order of a few nanometers [37]. Considering the typical water contact angle values measured on PP substrates, which are generally higher than 90° [36,38] and often exceed 110° depending on the type of PP (see, for example, the works by Long et al. [39] and Zhang et al. [40]), it is reasonable to assume a considerable increase in wettability due to the presence of GCC particles.

3.4. *Mechanical properties of bicomponent PP fibers*

The typical stress-strain curves for each fiber type are plotted in Fig. 9, while the average values of the main mechanical performance indices of the bicomponent PP fibers are summarized in Fig. 10. To allow a comprehensive comparison between the newly developed fibers presented here and those investigated in previous studies containing the same amount of 10 vol% filler but PCC instead of GCC [19] ($\sigma = 420 \pm 22.1$ MPa, $\varepsilon = 51 \pm 5.4$ %, $E = 3.8 \pm 0.3$ GPa), as well as the M-PP fibers, the highest possible drawing ratio of three was used, as detailed in Section 2.2. Unlike the PCC-filled fibers, which exhibited agglomerations that reduced their mechanical properties and processing efficiency, GCC-filled fibers showed improved homogeneity and mechanical performance. Therefore, for this study, the PCC filler was replaced with GCC filler, as GCC is also derived from natural stone.

In contrast to M-PP fiber, the tensile strength and stiffness of the B-PP fibers were more than doubled at the expense of a significant reduction in the strain at break, even though they indicate a lower degree of molecule chain orientation as GCC particles amount increases, as discussed in Section 3.2. This improvement was achieved through potential differences in raw PP type and spinning procedures between M-PP fibers and our B-PP fiber production. In addition, the stress-strain curves reveal that the mechanical properties of B-PP fibers decrease with increasing particle content due to non-uniform flow behavior of shell compound during melt-spinning, as presented in Table 2 by the MFR values. Despite this, they remain superior to the benchmark M-PP fiber, except for the B-40G PP fiber. This high particle content of 40 % by volume leads to an inhomogeneous surface, creating strain concentration points within the fibers. Consequently, the 'form fit' structure, which increase mechanical interlocking by enhancing adhesion capability in concrete, is compromised, resulting in reduced spinnability and overall fiber tensile strength. The extremely low strain of B-40G PP fibers indicate that a higher drawing ratio is not feasible.

3.5. *Pullout behavior*

To qualitatively and quantitatively evaluate the interfacial interaction resulting from the induced rough surfaces, single fiber pullout tests were conducted on the B-PP fibers, with the results displayed in Fig. 11 and Fig. 12. These were compared to the commercial M-PP fiber within a normal-strength concrete matrix. Results for M fibers have been presented in a previous paper by Popa *et al.* [19] and here reported as a benchmark. The pullout work for displacements of 100, 200 and 300 µm, denoted as W_{100}, W_{200} and W_{300}, was calculated considering fiber breakage at a minimum displacement of approximately 120 µm and end measurement at 300 µm displacement, as discussed in Section 2.2. The F_{max} values were calculated by averaging the results from 15 tests performed for each batch of fibers. The results are plotted in the bar chart of Fig. 10.

A notable increase in pullout work values was observed for the B-PP fibers compared to the M-PP fiber, consistent with previous studies [19] on different modification strategies. The enhanced mechanical interlocking is attributed to the increased surface micro roughness resulting from the addition of particles to the fiber shell.

The threshold at which the failure mode started shifting from pullout to fiber tensile breakage was represented by a fiber volume fraction of 20 % in the shell. This was due to the competing effects of tensile strength reduction and micro roughness increase. Moreover, increasing the particle content up to the arbitrarily chosen spinning limits (i.e. B-40G in Fig. 11d) resulted in a drastic drop in energy absorption capacity

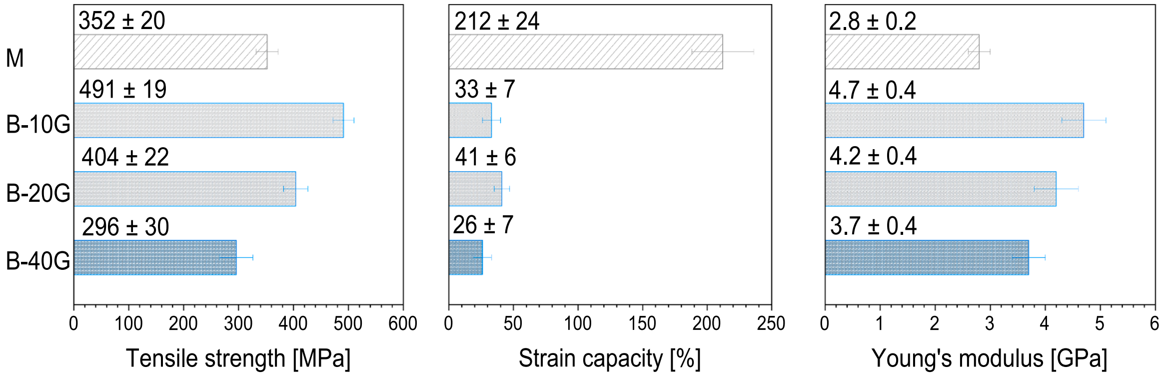

Fig. 10. Bar graphs illustrating the mechanical properties of the M-PP fiber vs. offline drawn (DR=3) B-PP fibers. Note the different limits of the scale axes.

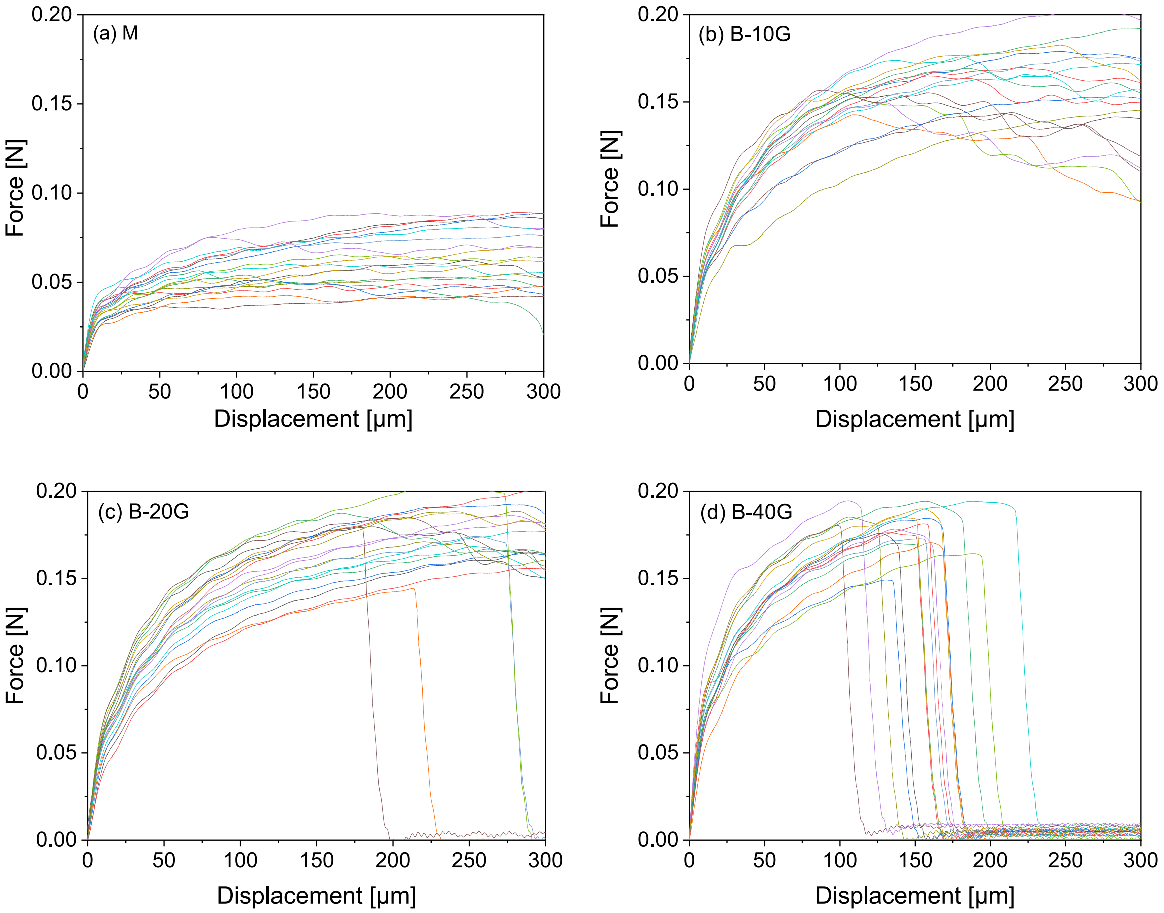

Fig. 11. Dynamic SFPO force-displacement curves of measurements at embedding length $l_e = 1000$ µm of the (a) M-PP fiber vs. the (b-d) offline drawn (DR=3) B-PP fibers pulled out of the normal strength matrix.

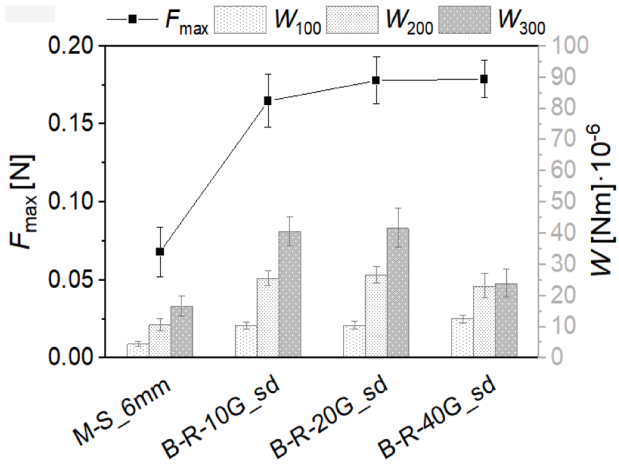

Fiber name	F_{max} [N]	W_{100}	W_{200}	W_{300}
		[Nm] · 10^{-6}		
M [19]	0.07 ±0.02	4.6 ± 0.8	10.7 ± 2.1	16.8 ± 3.2
B-10G	0.17 ± 0.02	10.5 ± 1.1	25.7 ± 2.4	40.7 ± 4.5
B-20G	0.18 ± 0.02	10.6 ± 1.2	26.6 ± 2.6	41.8 ± 6.2
B-30G	0.18 ± 0.01	12.6 ± 1.2	23.2 ± 3.9	24.0 ± 4.5

Fig. 12. Bar graphs and table illustrating the mean values of peak force F_{max} (black line plots) and the pullout work until 100, 200 and 300 µm displacement W_{100}, W_{200} and W_{300} (gray charts) and the standard deviations. Note the different limits of the scale axes.

compared to other B-PP fibers, owing to premature fiber breakage occurring at modest displacements. In fact, with respect to the other fiber types, the peak bond stress was rapidly reached due to the reduced transfer length promoted by the increased interlocking as indicated by Signorini *et al.* [41], followed by sudden fiber rupture of all B-40G PP fibers, at a displacement ranging from approximately 120 µm to 230 µm. Nevertheless, despite the observation of premature tensile failure of the fiber, the increased bond strength stemming from surface micro roughness amply compensates for the poor interfacial adhesion by M-PP fibers [19].

3.6. *Fiber surfaces after pullout*

The examination of the fibers' surface by SEM after the SFPO tests of M-PP fiber compared to the B-PP fibers is displayed in Fig. 13. The surface of M-PP fibers reveals only sparse, thin longitudinal lines

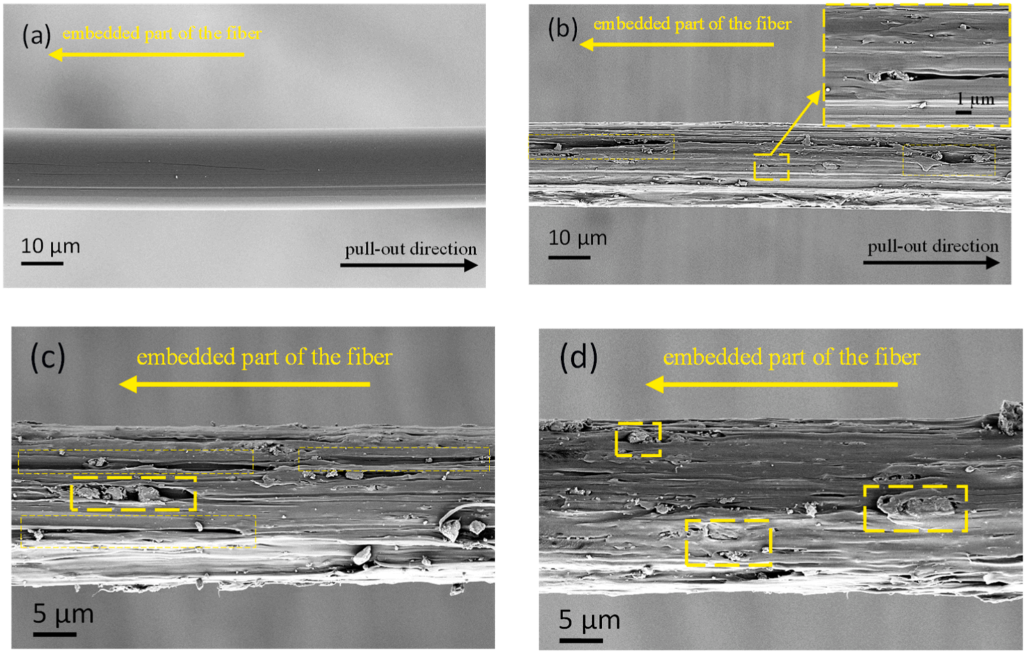

Fig. 13. SEM representative morphology images of the commercial monocomponent (M-PP) fiber, and bicomponent fibers, i.e. (b) B-10G PP and (c, d) B-20G PP fibers after being pulled out of the cementitious matrix.

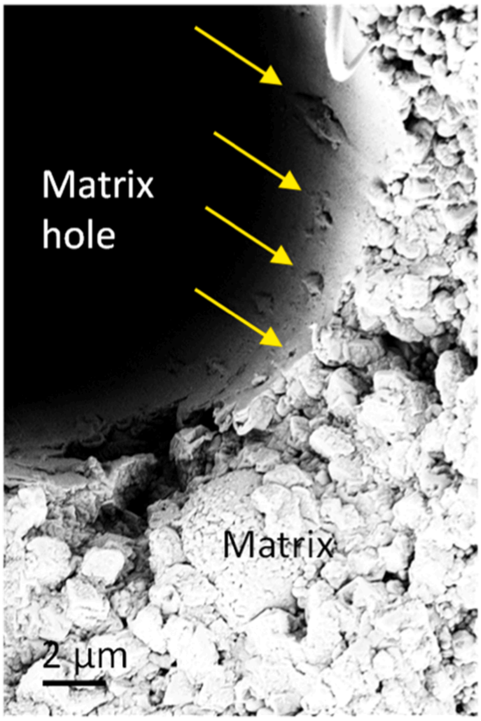

Fig. 14. SEM representative image of the embedment channel within the cementitious matrix after the complete B-20G PP fiber pullout. The yellow arrows point possible particle remnants that remain within the fiber-matrix interlocking zone.

resulting from polymer abrasion. This response is typical of a smooth, hydrophobic surface, such as plain polypropylene, and has been extensively documented in the literature [42–44]. The absence of chemical functional groups and roughness on the surface prevents fiber-matrix chemical bond and mechanical interlocking, allowing the fiber to slip without visible damage. Conversely, distinctive, pronounced deformation patterns are observed for bicomponent fiber types whose shell portion incorporates particles, as shown in Fig. 13b-d. Remarkably, both varieties of bicomponent PP fibers, incorporating either 10 % or 20 % $CaCO_3$ particles, exhibit the following: (i) longitudinal abrasions of the polymer medium from the surface, and (ii) displacement of the particles during extraction. The former phenomenon is evident in the form of thin scratches on the fiber surface, while the latter is characterized by *localized* micro-excavations of varying depths depending on the size and local agglomeration of the $CaCO_3$ particles, which are dragged and excavate through locking.

This rather localized, characteristic damage mode, known as the "*locking-front model*", is typically observed on hydrophilic polyvinyl alcohol (PVA) fiber surfaces, as documented in the study by Ranjbarian et al. [45], and significantly contributes to the increase in the pullout force during the post-debonding stage, which is often referred to as "*slip-hardening*" [42,46]. In addition, particles that moved along the fiber surface and remain embedded in the polymer can lead to plastic surface tearing deformation. This deformation is clearly visible in the magnified inlet of Fig. 13b, for example, and stems to the longitudinal, irreversible stretching of the PP shell layer.

To better understand the fiber-matrix interaction and the specific influence of adding GCC particles to the fiber shell, Fig. 14 illustrates the matrix channel where the fiber was positioned for the SFPO test. This micrograph shows a clear mechanical interlocking effect between the fiber and the matrix, which is underscored by the localized micro-grooving of the matrix and the potential presence of particle residues within the fiber-matrix interlocking zone, as indicated by the yellow arrows. This observation confirms the occurrence of a friction-driven interaction at the interface, evidenced by surface wear marks and the likely transfer of GCC particles from the fiber surface to the surrounding matrix during the pullout process.

These SEM observations directly relate to the fiber's slip and fracture behavior. In fact, the scratches and localized matrix deformation indicate stress transfer and resistance to fiber pullout, demonstrating how surface roughness and particle-induced interlocking enhance energy absorption and delay fiber slip.

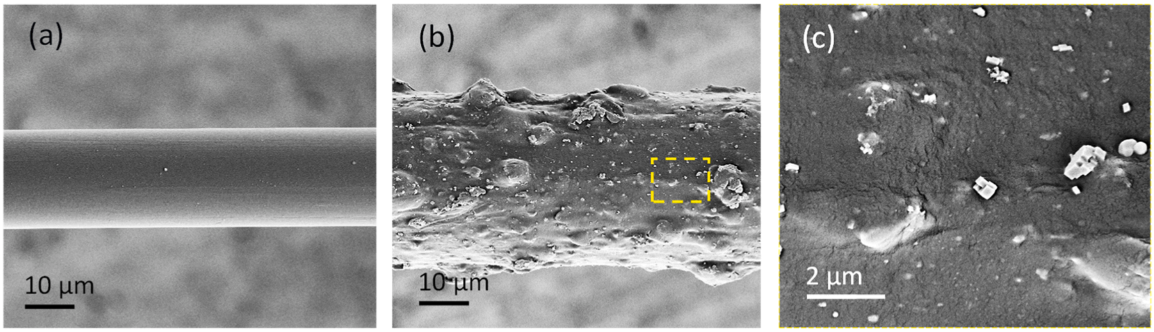

Fig. 15. SEM images of the (a) M-PP fiber and (b-c) as-spun B-20G PP fiber after 5 days in cementitious pore solution. Note the different limits of the scale axes.

3.7. Fiber surface modification after immersion in cementitious pore solution

The morphological change of the fibers after immersion in the cementitious pore solution and the possible nucleation of hydration products were examined by SEM analysis after five days of immersion (Fig. 15). As shown in Fig. 15a, no hydration products were detected on the inert M-PP fiber surface, confirming the poor wettability of plain PP [47,48]. Conversely, the as-spun B-20G PP counterpart (Fig. 15b,c) showed a uniform deposition of cement pore solution hydration products along the surface, resulting in a significantly increased development of crystal nucleation sites.

In the magnified view of the B-20C PP fiber surface in Fig. 15c, clusters of calcium carbonate (most likely in the polymorph of *calcite*) with distinct cubic hydrates were observed [49,50]. This study is restricted to 5 days of immersion and only provides insights into the improved hydrophilicity of this new variety of B-PP fibers. Further analysis is needed to provide a more comprehensive assessment of the hydration reactions occurring at the interface. In fact, according to Lakshtanov and Stipp [51], nucleation and growth mechanisms can influence the shape and size of the crystals formed. Nevertheless, a qualitative evidence of improved compatibility between the modified PP fiber and cementitious media can be provided, underlying a promising application in fiber-reinforced cementitious composites with enhanced bridging capacity of this class of engineered PP fibers.

4. Conclusions and outlook

To address issues with state-of-the-art fibers (M-PP), namely smooth surface, poor hydrophilicity, and weak matrix bonding, we have advanced the polypropylene development of bicomponent PP fibers. These novel fibers feature ground GCC particles in their outer shell, enhancing surface micro roughness for better interlocking in the concrete matrix. The main findings can be summarized as follows:

- A reduction in the size of the GCC particles, together with an optimization of compounding parameters could facilitate their incorporation into the fiber shell, thereby reducing the likelihood of clogging at the dies zone during the melt-spinning process.
- Increasing the GCC content in the fiber shell progressively reduced the mechanical properties of the single fiber. Despite this reduction, fibers with moderate filler content (B-20G) still outperformed commercial M-PP fibers typically used for fiber-reinforced concrete applications. The highest filler content (B-40G) led to inhomogeneous surface that failed prematurely, demonstrating lower tensile performance than commercial M-PP fibers.
- As emerged from SFPO tests, the onset of fiber breakage was observed with B-20G PP fibers, which subsequently progressed to complete fiber breakage with B-40G PP fiber. This latter fiber type exhibited slightly higher energy absorption than M-PP fiber. However, B-40G PP fiber showed a pronounced reduction in energy absorption compared to other B-PP fibers, experiencing nearly instantaneous failure at small displacements (approximately 120–230 µm) during SFPO tests. In contrast, fibers with moderate filler content in their shell offered a good balance of mechanical interlocking and controlled failure.
- In addition to improving the mechanical interlocking between the fiber and matrix, incorporating GCC particles into the fiber shell created nucleation sites for the formation of the hydration products of the cementitious phases upon immersion. This process was evidenced by crystal deposits on the fiber surface, facilitating the development of some extent of chemical bonding at the fiber–matrix interface. However, the characterization of the chemical fiber-matrix interaction was beyond the scope of the present study and is currently being investigated in greater detail.

In terms of economic assessment, while no specific prediction can be made at this stage, it is expected that the modified PP fibers will incur slightly higher costs, since the particles must be compounded in a PP matrix as an additional step. However, once the spinning process has been established, it does not differ from that of neat PP fibers, although it may run at a reduced velocity.

This micro-level study represents the basis for scaling up our research, optimizing variables such as particle content, melt-spinning investigation parameters, and polypropylene type for the production of bicomponent PP fibers. In addition, by improving the interfacial bond with mineral media, we aim to increase the tensile ductility of PP fiber-reinforced concrete composites, particularly with respect to impact loading. Future work will involve macro-scale testing, building on our previous studies [21].

Funding

The German Research Foundation (Deutsche Forschungsgemeinschaft – DFG) within the framework of the Research Training Group GRK 2250/2 'Mineral-bonded composites for enhanced structural impact safety' funds this research project number 287321140.

CRediT authorship contribution statement

Christina Scheffler: Validation, Supervision, Project administration, Funding acquisition, Conceptualization. **Viktor Mechtcherine:** Writing – review & editing, Supervision, Funding acquisition. **Cesare Signorini:** Writing – review & editing, Visualization, Validation, Methodology. **Mihaela-Monica Popa:** Writing – original draft, Visualization, Methodology, Investigation, Formal analysis, Data curation, Conceptualization. **Norbert Smolka:** Writing – review & editing, Methodology.

Declaration of Competing Interest

The authors declare that they have no known competing financial interests or personal relationships that could have appeared to influence the work reported in this paper.

Acknowledgments

The authors wish to express their gratitude to Ms. Steffi Preßler for her assistance with sample preparation and the execution of single-fiber pullout tests and SEM investigations as well as to Ms. Maria auf den Landwehr for conducting SEM-EDX investigations. Additional thanks go to Ms. Christine Steinbach for her work on particle size distribution analysis and to Dr. Ahmad Chihadeh for Python coding for pullout test calculations.

Data availability

Data will be made available on request.

References

[1] V. Mechtcherine, F. De Andrade Silva, M. Butler, D. Zhu, B. Mobasher, S.L. Gao, et al., Behaviour of strain-hardening cement-based composites under high strain rates, J. Adv. Concr. Technol. 9 (2011) 51–62, https://doi.org/10.3151/jact.9.51.

[2] E.-H. Yang, V.C. Li, Tailoring engineered cementitious composites for impact resistance, Cem. Concr. Res. 42 (2012) 1066–1071, https://doi.org/10.1016/j.cemconres.2012.04.006.

[3] C. Signorini, F. Bracklow, M. Hering, M. Butler, L. Leicht, T. Schubert, et al., Ballistic limit and damage assessment of hybrid fibre-reinforced cementitious thin composite plates under impact loading, J. Build. Eng. 80 (2023) 108037, https://doi.org/10.1016/j.jobe.2023.108037.

[4] T. Kanda, V.C. Li, Effect of Fiber Strength and Fiber-Matrix Interface on Crack Bridging in Cement Composites, J. Eng. Mech. 125 (1999) 290–299, https://doi.org/10.1061/(ASCE)0733-9399(1999)125:3(290).

[5] R. Ranade, V.C. Li, W.F. Heard, Tensile Rate Effects in High Strength-High Ductility Concrete, Cem. Concr. Res. 68 (2015) 94–104, https://doi.org/10.1016/j.cemconres.2014.11.005.

[6] I. Curosu, V. Mechtcherine, O. Millon, Effect of fiber properties and matrix composition on the tensile behavior of strain-hardening cement-based composites (SHCCs) subject to impact loading, Cem. Concr. Res. 82 (2016) 23–35, https://doi.org/10.1016/j.cemconres.2015.12.008.

[7] C. Suksiripattanapong, T. Phetprapai, W. Singsang, C. Phetchuay, J. Thumrongvut, W. Tabyang, Utilization of Recycled Plastic Waste in Fiber Reinforced Concrete for Eco-Friendly Footpath and Pavement Applications, Sustainability 14 (2022) 6839, https://doi.org/10.3390/su14116839.

[8] C. Signorini, A. Nobili, Durability of fibre-reinforced cementitious composites (FRCC) including recycled synthetic fibres and rubber aggregates, Appl. Eng. Sci. 9 (2022) 100077, https://doi.org/10.1016/J.APPLES.2021.100077.

[9] C. Signorini, A. Sola, B. Malchiodi, A. Nobili, Highly Dissipative Fiber-Reinforced Concrete for Structural Screeds, J. Mater. Civ. Eng. 34 (2022) 04022022, https://doi.org/10.1061/(ASCE)MT.1943-5533.0004160.

[10] R.R. Patil, V.D. Katare, Application of fiber reinforced cement composites in rigid pavements: A review, Mater. Today. Proc. (2023) S2214785323023167, https://doi.org/10.1016/j.matpr.2023.04.415.

[11] F. Salaün, G. Creach, F. Rault, X. Almeras, Thermo-physical properties of polypropylene fibers containing a microencapsulated flame retardant, Polym. Adv. Technol. 24 (2013) 236–248, https://doi.org/10.1002/pat.3076.

[12] M. Leskovšek, G. Jedrinović, Elesini U. Stankovic, Properties of polypropylene fibres with incorporated microcapsules, Acta Chim. Slov. 51 (2004) 699–715.

[13] K. Iqbal, D. Sun, Development of thermal stable multifilament yarn containing micro-encapsulated phase change materials, Fibers Polym. 16 (2015) 1156–1162, https://doi.org/10.1007/s12221-015-1156-9.

[14] G. Fredi, H. Bruenig, R. Vogel, C. Scheffler, Melt-spun polypropylene filaments containing paraffin microcapsules for multifunctional hybrid yarns and smart thermoregulating thermoplastic composites, Express Polym. Lett. 13 (2019) 1071–1087, https://doi.org/10.3144/expresspolymlett.2019.93.

[15] W. Wei, E. Shim, W. Barnes, B. Pourdeyhimi, Structure–property relationship of melt spinning polypropylene fibers containing inorganic particulate CaCO3 fillers, Text. Res. J. 91 (2021) 1419–1435, https://doi.org/10.1177/0040517520982001.

[16] A. Ariffin, S.S. Jikan, M.S.F. Samsudin, Z.M. Ariff, Z.A.M. Ishak, Melt Elasticity Phenomenon of Multicomponent (Talc and Calcium Carbonate) Filled Polypropylene, J. Reinf. Plast. Compos. 25 (2006) 913–923, https://doi.org/10.1177/0731684406063550.

[17] M.M. Popa, H. Brünig, I. Curosu, V. Mechtcherine, C. Scheffler, Spinability and characteristics of particle-shell PP-bicomponent fibers for crack bridging in mineral-bonded composites. RILEM Bookseries, Springer Science and Business Media B.V, 2022, pp. 255–264, https://doi.org/10.1007/978-3-030-83719-8_23.

[18] E. Wölfel, H. Brünig, I. Curosu, V. Mechtcherine, C. Scheffler, Dynamic Single-Fiber Pull-Out of Polypropylene Fibers Produced with Different Mechanical and Surface Properties for Concrete Reinforcement, Materials 14 (2021) 722, https://doi.org/10.3390/ma14040722.

[19] M.-M. Popa, A. Leuteritz, M. Stommel, I. Kühnert, V. Mechtcherine, C. Scheffler, Micromechanical study on polypropylene-bicomponent fibers to improve mechanical interlocking for application in strain-hardening cement-based composites, Cem. Concr. Compos. 142 (2023) 105181, https://doi.org/10.1016/j.cemconcomp.2023.105181.

[20] M.M. Popa, A. Leuteritz, M. Stommel, V. Mechtcherine, C. Scheffler, Treatments of polypropylene bicomponent fibers to optimize their interlocking in concrete by micro-CaCO3 particle addition. Applications and Structures: 20th European Conference on Composite Materials: Composites Meet Sustainability, ECCM 2022, Composite Construction Laboratory (CCLab), Ecole Polytechnique Federale de Lausanne (EPFL), 2022, pp. 547–554.

[21] M.-M. Popa, C. Signorini, M.A.B. Beigh, A. Chihadeh, M. Stommel, M. Kaliske, et al., Bond and cracking behavior of tailored limestone calcined clay cement-based composites including bicomponent polypropylene fibers with enhanced mechanical interlocking, Cem. Concr. Compos. 155 (2025) 105812, https://doi.org/10.1016/j.cemconcomp.2024.105812.

[22] L. Hong, Y.D. Chen, T.D. Li, P. Gao, L.Z. Sun, Microstructure and bonding behavior of fiber-mortar interface in fiber-reinforced concrete, Constr. Build. Mater. 232 (2020) 117235, https://doi.org/10.1016/j.conbuildmat.2019.117235.

[23] M.-M. Popa, A.H. Ahmed, C. Signorini, V. Mechtcherine, C. Scheffler, Impact-Response of Tailored Composites Made of Novel Polypropylene Fibers in a Low-Clinker LC3 Matrix, in: V. Mechtcherine, C. Signorini, D. Junger (Eds.), Transforming Construction: Advances in Fiber Reinforced Concrete, 54, Springer Nature Switzerland, Cham, 2024, pp. 581–588, https://doi.org/10.1007/978-3-031-70145-0_70.

[24] I. Kuehnert, Y. Spoerer, H. Brünig, N.H.A. Tran, N. Rudolph, Processing of Poly (lactic Acid), Adv. Polym. Sci. (2017), https://doi.org/10.1007/12_2017_30.

[25] Jr R.D.H., Parker J.P., King C.L. Method for making bicomponent fibers. US4552603A, 1985.

[26] Praxis der Thermischen Analyse von Kunststoffen | Hanser-Fachbuch n.d. ⟨https://www.hanser-fachbuch.de/fachbuch/artikel/9783446223400⟩ (accessed May 28, 2024).

[27] ASTM International - ASTM D1577-07(2018) - Standard Test Methods for Linear Density of Textile Fibers | Engineering360 n.d. ⟨https://standards.globalspec.com/std/13000126/astm-d1577-07-2018⟩ (accessed October 19, 2021).

[28] Dissertation_E_Woelfel.pdf n.d.

[29] BS 2955:1993 | 15 May 1993 | BSI Knowledge n.d. ⟨https://knowledge.bsigroup.com/products/glossary-of-terms-relating-to-particle-technology?version=standard⟩ (accessed April 25, 2024).

[30] Chew N.Y.K., Chan H.-K. Effect of Powder Polydispersity on Aerosol Generation 2002.

[31] W.C.J. Zuiderduin, C. Westzaan, J. Huétink, R.J. Gaymans, Toughening of polypropylene with calcium carbonate particles, Polymer 44 (2003) 261–275, https://doi.org/10.1016/S0032-3861(02)00769-3.

[32] (PDF), Polypropylene chain scissions and molecular weight changes in multiple extrusion. ResearchGate, 2024, https://doi.org/10.1016/S0141-3910(96)00233-9.

[33] M. Al-Samhan, F. Al-Attar, J. Al-Fadhli, M. Al-Shamali, The Influence of Nano CaCO3 on Nucleation and Interface of PP Nano Composite: Matrix Processability and Impact Resistance, Polym. (Basel) 13 (2021) 1389, https://doi.org/10.3390/polym13091389.

[34] H. Mao, B. He, W. Guo, L. Hua, Q. Yang, Effects of Nano-CaCO3 Content on the Crystallization, Mechanical Properties, and Cell Structure of PP Nanocomposites in Microcellular Injection Molding, Polym. (Basel) 10 (2018) 1160, https://doi.org/10.3390/polym10101160.

[35] K.J. Stout, The Development of methods for the characterisation of roughness in three dimensions, Comm. Eur. Communities Luxemb. (1993) 130.

[36] F. Huang, Q. Wei, X. Wang, W. Xu, Dynamic contact angles and morphology of PP fibres treated with plasma, Polym. Test. 25 (2006) 22–27, https://doi.org/10.1016/j.polymertesting.2005.09.017.

[37] J. Long, P. Chen, Surface Characterization of Hydrosilylated Polypropylene: Contact Angle Measurement and Atomic Force Microscopy, Langmuir 17 (2001) 2965–2972, https://doi.org/10.1021/la001547u.

[38] Q.F. Wei, R.R. Mather, A.F. Fotheringham, R.D. Yang, ESEM Study of Wetting of Untreated and Plasma Treated Polypropylene Fibers, J. Ind. Text. 32 (2002) 59–66, https://doi.org/10.1106/152808302031066.

[39] X. Long, L. He, Y. Zhang, S. Yu, M. Ge, Surface modification of polypropylene non-woven fabric for improving its hydrophilicity, Surf. Eng. 34 (2018) 818–824, https://doi.org/10.1080/02670844.2018.1429205.

[40] H. Zhang, L. Zhang, X. Han, L. Kuang, D. Hua, Guanidine and Amidoxime Cofunctionalized Polypropylene Nonwoven Fabric for Potential Uranium Seawater Extraction with Antifouling Property, Ind. Eng. Chem. Res 57 (2018) 1662–1670, https://doi.org/10.1021/acs.iecr.7b04687.

[41] C. Signorini, A. Nobili, M. Liebscher, J. Zhao, A.H. Ahmed, T. Köberle, et al., Assessing the stress-transfer capability of mineral impregnated PBO yarns in a limestone calcined clay cement-based (LC3) matrix, Composites Part B Engineering 276 (2024) 111364, https://doi.org/10.1016/j.compositesb.2024.111364.

[42] A. Sorzia, C. Signorini, V. Volpini, P. Di Maida, Analytical Approach for Modelling the Pull-Out Mechanism of Recycled Synthetic Fibres in Fibre-Reinforced Concrete (FRC), KEM 919 (2022) 35–46, https://doi.org/10.4028/p-4k539k.

[43] M. Ahsani, R. Yegani, Study on the fouling behavior of silica nanocomposite modified polypropylene membrane in purification of collagen protein, Chem. Eng. Res. Des. 102 (2015) 261–273.

[44] A. Peled, E. Zaguri, G. Marom, Bonding characteristics of multifilament polymer yarns and cement matrices, Composites Part A Applied Science Manufacturing 39 (2008) 930–939, https://doi.org/10.1016/j.compositesa.2008.03.012.

[45] M. Ranjbarian, V. Mechtcherine, Z. Zhang, I. Curosu, J. Storm, M. Kaliske, Locking Front Model for pull-out behaviour of PVA microfibre embedded in cementitious matrix, Cem. Concr. Compos. 103 (2019) 318–330, https://doi.org/10.1016/j.cemconcomp.2019.04.031.

[46] A. Sorzia, L. Lanzoni, E. Radi, Pullout modelling of viscoelastic synthetic fibres for cementitious composites, Compos. Struct. 223 (2019) 110898, https://doi.org/10.1016/j.compstruct.2019.110898.

[47] H. R. Pakravan, M. Jamshidi, M. Latifi, Adhesion of Polypropylene Fiber to Cement Matrix, J. Adhes. Sci. Technol. 26 (2012) 1383–1393, https://doi.org/10.1163/156856111X618263.

[48] C. Signorini, V. Volpini, Mechanical Performance of Fiber Reinforced Cement Composites Including Fully-Recycled Plastic Fibers, Fibers 9 (2021) 16, https://doi.org/10.3390/fib9030016.

[49] D. Kralj, J. Kontrec, L. Brečević, G. Falini, V. Nöthig-Laslo, Effect of Inorganic Anions on the Morphology and Structure of Magnesium Calcite, Chem. A Eur. J. 10 (2004) 1647–1656, https://doi.org/10.1002/chem.200305313.

[50] D. Ergenç, R. Fort, Accelerating carbonation in lime-based mortar in high CO2 environments, Constr. Build. Mater. 188 (2018) 314–325, https://doi.org/10.1016/j.conbuildmat.2018.08.125.

[51] L. Lakshtanov, S. Stipp, Interaction between dissolved silica and calcium carbonate: 1. Spontaneous precipitation of calcium carbonate in the presence of dissolved silica, Geochim. Et. Cosmochim. Acta 74 (2010) 2655–2664, https://doi.org/10.1016/j.gca.2010.02.009.